http://dx.doi.org/10.21577/0103-5053.20180128

J. Braz. Chem. Soc., Vol. 29, No. 12, 2496-2501, 2018
Printed in Brazil - ©2018 Sociedade Brasileira de Química

Article

Synthesis and Optical Properties of Water-Soluble CdTe:Zn^{2+} Quantum Dots Prepared by the One-Pot Approach

José C. L. Sousa,[a] Marcelo G. Vivas,[b] Jefferson L. Ferrari[a] and Marco A. Schiavon[*,a]*

[a]*Departamento de Ciências Naturais, Universidade Federal de São João Del-Rei, Campus Dom Bosco, Praça Dom Helvécio, 74, 36301-160 São João Del-Rei-MG, Brazil*

[b]*Instituto de Ciência e Tecnologia, Universidade Federal de Alfenas, Cidade Universitária, BR 267, km 533, 37715-400 Poços de Caldas-MG, Brazil*

This paper reports the synthesis and characterization of ternary CdTe:Zn^{2+} quantum dots (QDs) passivated with reduced *L*-glutathione (GSH) dispersed in water. The synthesis was performed through a one-pot approach and their size-dependent optical properties were investigated through steady-state absorption and emission spectroscopies along with the evolving factor analysis/multivariate curve resolution alternating least squares (EFA/MCR-ALS) method. Our results show that the incorporation of Zn^{2+} ions in CdTe:Zn^{2+} QDs, during the synthesis time, decreases the CdTe:Zn^{2+} QDs predominant diameter in the ensemble and increases their size dispersion. In addition, fluorescence quantum yield measurements suggest a reduction in the number of surface defects in CdTe:Zn^{2+} QDs as compared with CdTe QDs, when both are produced from the same synthesis route.

Keywords: CdTe:Zn^{2+}, quantum dots, nanocrystals, alloys

Introduction

In the last few decades, nanostructured materials, such as fullerenes, nanotubes, nanoribbons, nanowires and nanocrystals (NCs), have attracted great attention due to their remarkable optical and electronic properties. In particular, semiconductor NCs, crystalline structures that can be confined in one, two or three spatial dimensions with length varying from 1 to 100 nm,[1,2] present special optical features related to the strong confinement effect of electrons, which occurs when the NC radius becomes smaller than the Bohr radius.[3,4] Materials that exhibit a system of electrons confined in all three spatial dimensions have quantized energy levels, such as atoms and molecules. Such systems are called artificial atoms or quantum dots (QDs). Nowadays, QDs are active materials used in several kinds of applications, such as solar cells, electronic and photonics devices, fluorescence probes, to cite a few, due to their size-dependent optical properties.[5-8] For example, for colloidal semiconductor QDs, the smaller the dot size the higher the electron-hole pair (exciton) recombination energy. Consequently, one can tune the QDs optical responses from UV to near infrared region by changing only its size.[9-12]

II-VI semiconductor QDs represent one of the most important types of nanomaterials.[13-17] One common characteristic of all nanostructures is the high ratio of surface area/volume as compared with bulk materials. Therefore, surface chemistry and polydispersity are the factors that most influence the heterogeneity of the optical properties of QDs.[18,19] Although QDs can be applied in photovoltaic industries, thermal or light-emitting diodes, its applications in life sciences have revolutionized the state of the art of some biological assays, including fluorescence-linked immunosorbent assays (FLISA),[20] fluorescence resonance energy transfer (FRET) assays,[21] immunosensors,[22] DNA probes[23] or multicolor imaging dyes,[24] commonly being a real alternative to the use of traditional organic dyes. In this context, great effort has been made to synthesize novel nanomaterials, in particular, QDs with high surface quality and biocompatible ability, to enhance and fine tune the optical response, concomitantly becoming less harmful to human health.[25,26] A commonly used method for this purpose is to modify the capping molecule, which acts to reduce the surface defects and toxicity.[26] Another method is based on the introduction of transition elements like

*e-mail: schiavon@ufsj.edu.br

zinc into the QDs structure.[27,28] Thus, ternary CdTe:Zn^{2+} QDs passivated with *L*-glutathione (GSH) surface binding dispersed in water have been synthesized and characterized. The synthesis was performed through a one-pot approach, using the procedure described by Wang and Liu.[29] To aid in understanding the structure and optical properties relationship, we have performed steady-state absorption and emission spectroscopies, along with the evolving factor analysis/multivariate curve resolution alternating least squares (EFA/MCR-ALS) method.[30,31] Through this methodology, we have investigated the optical features, such as steady-state absorption and emission, fluorescence quantum yield (FQY) and size dispersion as a function of synthesis time. Our results pointed out that with the incorporation of Zn^{2+} ions in CdTe:Zn^{2+} QDs the QD predominant diameter in the ensemble decreases and their size dispersion concomitantly increases. We interpreted these results in light of the Ostwald ripening mechanism.[32,33] At the same time, our results indicate that there is a reduction in the number of surface defects in CdTe:Zn^{2+} QDs as compared with CdTe QDs produced from the same synthesis route.

Experimental

Chemicals

$CdCl_2.H_2O$ (99%; lot 0501337) was purchased from Vetec. $Zn(NO_3)_2$ (98%; lot S80603-359), GSH (98%; lot SLBB3118V), Na_2TeO_3 (99%; lot MKBG7198V) and rhodamine 6G (lot 04718TH) were obtained from Sigma-Aldrich. $NaBH_4$ (99%; lot 0471BJH) was purchased from Fluka. All chemicals were used as received, without further purification. Ultrapure water (type I) was used for experiments.

Synthesis of GSH-capped CdTe:Zn^{2+} QDs

The synthesis method used was modified from Wang and Liu.[29] Briefly, 0.427 mmol $CdCl_2.H_2O$ and 0.067 mmol $Zn(NO_3)_2$ were diluted in 80 mL ultrapure water in a 100 mL beaker. GSH (0.52 mmol) was added while stirring, followed by adjusting the pH to 10.0 with a solution of 1.0 mol L^{-1} of NaOH. Then, this solution was added to a 100 mL three-neck flask with a reflux column and a thermocouple coupled with a thermal heater (Cole-Parmer) to control the temperature. Then, 0.04 mmol Na_2TeO_3 and 1.0 mmol $NaBH_4$ were added to the solution, followed by reflux at 100 °C for up to 120 min. Aliquots were taken out at different time intervals and used to record the UV-Vis and photoluminescence (PL) spectra.

Characterization

The Zn:Cd molar ratio was measured by atomic absorption spectrophotometry (Varian Spectra AA 20). UV-Vis absorption and fluorescence spectra were acquired on a Shimadzu UV-2550 spectrophotometer and Shimadzu RF-5301 PC fluorimeter, respectively. Absorption and fluorescence measurements were performed with 10 mm quartz cuvettes using air-saturated solutions at room temperature. The FQYs of the nanocrystals were estimated using the fluorescence spectrum of the samples and a reference method described in detail by Kubin and Fletcher.[34] Here, we have used rhodamine 6G dissolved in water as the standard fluorescent dye (QY = 92%). The X-ray diffraction (XRD) pattern was obtained on a XRD-6000 (Shimadzu) using CuKα radiation, and the Fourier transform infrared (FTIR) spectra of samples were recorded using a Spectrum GX spectrophotometer (PerkinElmer), operating between 4000 and 400 cm^{-1}.

Results and Discussion

Figure 1 depicts the absorbance and fluorescence spectra for five (CdTe:Zn^{2+})-GSH samples with different synthesis times. The steady-state absorption spectra (Figure 1a) illustrate the first excitonic transition $1S_{3/2}(h) \rightarrow 1S(e)$, which is a function of QD size. This transition undergoes a considerable red shift of approximately 264 meV, indicating an increase in dots size during the course of the synthesis (from 15 to 120 min). The same behavior was observed for the fluorescence spectra (Figure 1b) excited at the wavelength corresponding to the $1S_{3/2}(h) \rightarrow 1S(e)$ transition of each QD sample. At the same time, an increase in fluorescence intensity was observed. However, the fluorescence measurements were performed at different concentrations, for instance, we used 14 μM for the QDs synthesized for 15 min and 5.5 μM for 120 min. It is worth mentioning that, as shown in Figure 1, the incorporation of Zn^{2+} ions in CdTe QDs does not modify the line shape of the absorption and emission spectra. The same result was found in Wang *et al.*[28] and, according to them, the diameters obtained through the high-resolution transmission electronic microscopy (TEM) are consistent with the results obtained from Yu's formula for CdTe QDs.[35] In this way, we can use the empirical relation obtained by Yu *et al.*[35] to estimate the average diameter for the (CdTe:Zn^{2+})-GSH samples and verify the influence of Zn^{2+} on their size-dependent optical properties.

In addition, we have estimated the band gap for the (CdTe:Zn^{2+})-GSH samples using the method described in the literature[36,37] (data not shown). Comparing these

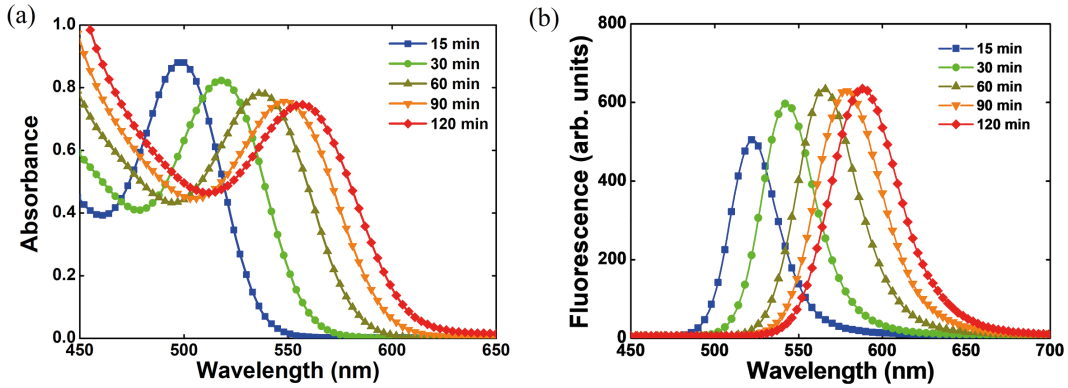

Figure 1. Evolution of the (a) absorption and (b) fluorescence spectra for GSH-capped CdTe:Zn^{2+} dispersions excited at the peak of absorption band related with the first excitonic transition.

results with those found for CdTe-GSH QDs of the same diameter,[19] it is noted that the band gap values are slightly higher in the presence of Zn^{2+} with increasing magnitude of 0.01, 0.04 and 0.05 eV for diameters 2.8, 3.1 and 3.3 nm, respectively. This outcome is also indicative of Zn^{2+} incorporation into the CdTe QDs.

To evaluate an interaction of the GSH ligand with an inorganic part of the nanoparticles, we have performed FTIR spectroscopy. Figure 2 shows the FTIR spectra for GSH, CdTe-GSH and (CdTe:Zn^{2+})-GSH. As can be seen, the FTIR spectra of the QDs stabilized with GSH are mainly characterized by pronounced IR absorption bands that occur between 3500 and 3000 cm^{-1} (ν_{OH}, ν_{NH}), and peaks at 1562 cm^{-1} (ν_{asym}C–O) and 1397 cm^{-1} (ν_{sym}C–O) are consistent with the fact that the carboxylic acid group is deprotonated at pH 10. The S–H vibrations (2525 cm^{-1}) are not detectable in the IR spectra of any of CdTe-GSH and (CdTe:Zn^{2+})-GSH bound ligands, which is expected for thiols covalently bound to the surface of the nanocrystals.[38-41] Furthermore, we did not observe a big difference between the FTIR spectra for CdTe-GSH and (CdTe:Zn^{2+})-GSH samples.

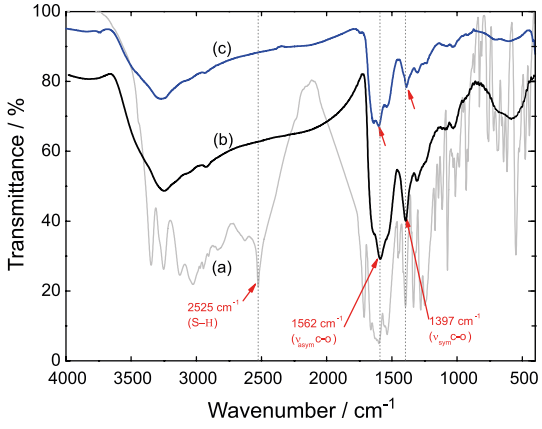

Figure 2. FTIR spectra of (a) free GSH, (b) GSH-capped CdTe QDs, (c) GSH-capped CdTe:Zn^{2+} QDs.

We have also performed XRD to check the dominant crystal phase. Figure 3 illustrates the XRD pattern of CdTe bulk and (CdTe:Zn^{2+})-GSH QDs. The XRD pattern for (CdTe:Zn^{2+})-GSH is characterized by a broad peak at ca. 40° (2θ), characteristic of CdTe QDs. In addition, the peaks for (CdTe:Zn^{2+})-GSH QDs match well with the bulk phase of CdTe, suggesting that the nanocrystals belong to the cubic zinc blende structure.

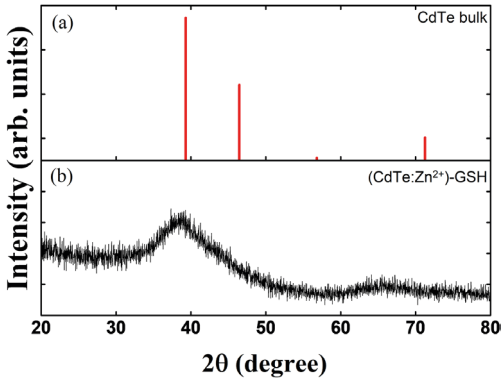

Figure 3. XRD pattern for (a) CdTe bulk and (b) (CdTe:Zn^{2+})-GSH QDs.

Figure 4 shows the increase of the QDs average diameter from 2.29 to 3.30 nm during the course of the synthesis (from 15 to 120 min).

As previously described, the optical properties for semiconductor QDs are size-dependent and, therefore, determining its average size is extremely important. Here, as mentioned, we have used the methodology described by Yu *et al.*[35] to determine the average size of the five (CdTe:Zn^{2+})-GSH samples. Therefore, all QDs synthesized (diameter < 4 nm) exhibit a very strong quantum confinement effect because the exciton Bohr radius for CdTe QDs is ca. 7.5 nm.[42] According to Figure 4, a great growth rate of QDs is predominant in the first 60 min (1.75×10^{-2} nm min^{-1}), and with longer times it undergoes a great reduction (3.7×10^{-3} nm min^{-1}). This outcome is

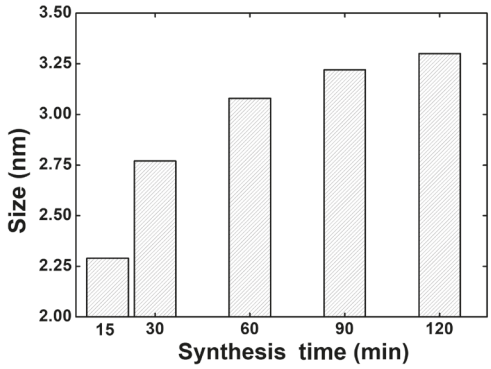

Figure 4. Synthesis time *vs.* size of CdTe:Zn^{2+} QDs.

characteristic of colloidal QDs synthesis, which is driven by the Ostwald ripening mechanism.[43]

Figure 5a illustrates the correlation between the dot size and fluorescence maximum position (FMP) parameter, while Figure 5b shows the correlation between the FQY and the QDs average diameter. For that, we have used the methodology described in the literature[44] and rhodamine 6G dissolved in water as standard sample.[34] The solid line in Figure 5a represents the fitting curve used to model FQY for GSH-capped CdTe:Zn^{2+} QDs with different sizes. In Figure 5b it is observed that the FQY reached a maximum of ca. 36% at 60 min and subsequently reduced at longer times, suggesting an increase in the number of defects on the QD surface, as previously reported.[45,46]

This is also a typical behavior of colloidal synthesis as in the one-pot method used in the present work. Moreover, the (CdTe:Zn^{2+})-GSH QDs exhibit higher FQY than CdTe QDs obtained from the same synthesis route,[19] even for the larger QDs. According to He and co-workers,[42] CdTe QDs exhibit oxidized Te surface sites that enhanced the nonradiative electron-hole recombination pathways, decreasing FQY. A possible explanation for this process has been suggested,[42] in which the authors describe that the Zn^{2+} ions in CdTe:Zn^{2+} QDs act in recovering the defect sites (oxidized Te), which generate improvements in the quality of the QDs' surface and, consequently, increases FQY.

To gain more information about (CdTe:Zn^{2+})-GSH QDs ensemble, we measured the fluorescence spectra after stepwise excitation (intervals of 2 nm) at all wavelengths along the lowest energy excitonic band of the QDs. In Figure 6a, we show graphs (color maps) of the emission *vs.* excitation wavelengths obtained for each synthesis time. The first aspect to highlight is that depending on the excitation wavelength, we observed different regions of emission. This occurs because the sample has an ensemble of QDs with distinct sizes. Nevertheless, each QD emits at a particular wavelength, as shown in Figure 6a, and, therefore, we observed a specific range of emission wavelengths for each sample. The second aspect is related to the increase in synthesis time (and consequent increase of QDs average size) that induces a red shift in the range of emission wavelengths, which can be easily visualized in Figure 6a (displacement of the emission region along the horizontal axis).

From Figure 6a, we employed the EFA/MCR-ALS method[47] to determine the predominant QD diameters in the ensemble for each synthesis time. This method makes a decomposition of all the QDs' fluorescence spectra excited along the lowest energy absorption band and through a specific iterative procedure determines the predominant QD diameter in the ensemble. Details about this method can be found in Mutavdzic *et al.*[48] Figure 6b depicts the normalized emission spectra obtained from the EFA/MCR-ALS analysis for each synthesis time indicating the predominant QD diameters in the ensemble. According to this method, all samples have four predominant QD diameters (see number of spectra in Figure 6b). However, three of them have the same diameter within the experimental error. Therefore, according to EFA/MCR-ALS analysis, the predominant QD diameters were 2.09 and 2.30 nm for 15 min, 2.53 and 2.75 nm for 30 min, 2.91 and 3.06 nm

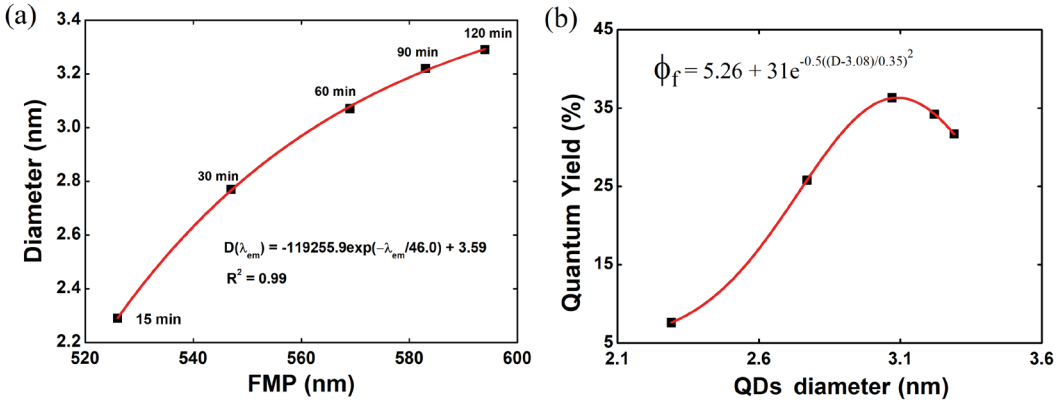

Figure 5. (a) Size/FMP dependence and (b) fluorescence quantum yield *vs.* average diameter for GSH-capped CdTe:Zn^{2+} QDs.

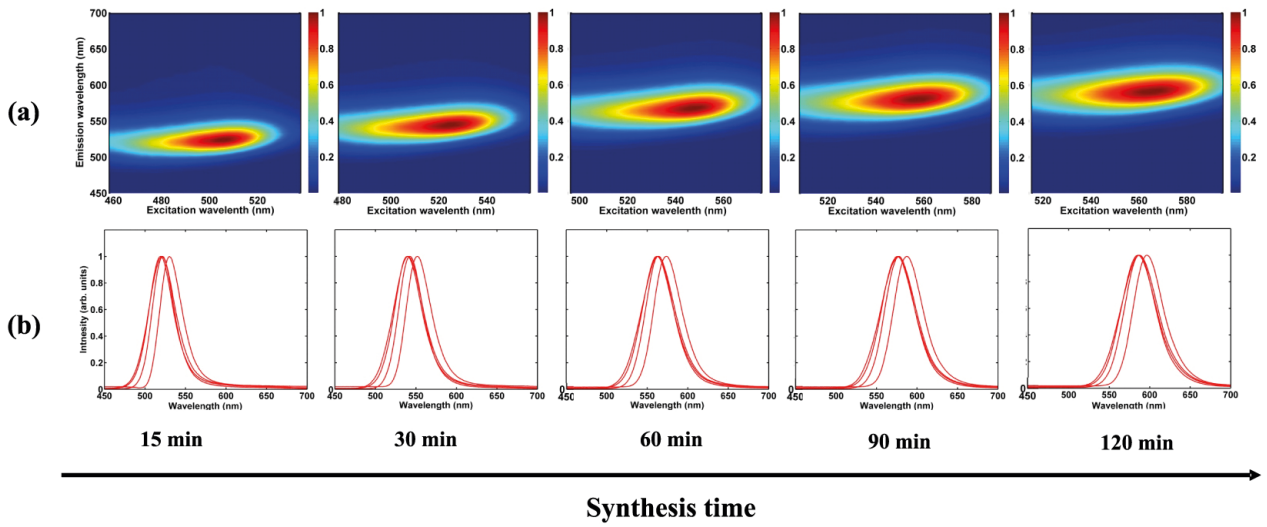

Figure 6. (a) Color map representing the emission *vs.* excitation wavelengths for each synthesis time; (b) normalized characteristic emission spectra obtained from the EFA/MCR-ALS method for each QDs solution.

for 60 min, 3.10 and 3.20 nm for 90 min, and 3.20 and 3.27 nm for 120 min.

If we compare these results with the ones obtained through the same synthesis route for GSH-capped CdTe[19] we observe a reduction of approximately 10% in predominant QD diameter in each sample. This result suggests that the incorporation of the Zn^{2+} ions causes a reduction in predominant QD diameters in ensemble. Moreover, from the EFA/MCR-ALS analysis, an increase in the range of the predominant QD diameters (related to the increase of size dispersion) is observed for CdTe:Zn^{2+} as compared with the CdTe produced from the same synthesis route. Finally, both effects (decrease of average size and increase of size dispersion) seem to be associated with the reduction in number of surface defects occasioned by the Zn^{2+} ions. It is worthwhile to remember that the Zn^{2+} ionic radius (60 pm) is smaller than the Cd^{2+} ionic radius (78 pm); this makes it possible for zinc ion to be incorporated into the CdTe crystalline structure,[49] in addition to the possible interaction on the surface.

Conclusions

Here, we have synthesized and reported the optical properties for five samples of (CdTe:Zn^{2+})-GSH QDs dispersed in water containing different average sizes and dispersions. We observed that the incorporation of Zn^{2+} ions in (CdTe:Zn^{2+})-GSH QDs decreases the predominant diameter in the ensemble and increases their size dispersion as we compared them with CdTe-GSH QDs synthesized using the same synthesis route.[19] Another significant outcome reported here is that the presence of Zn^{2+} ions increases the FQY in relation to QDs synthesized in the absence of metal, most probably because Zn^{2+} ions reduce the surface defects, even for larger QDs. All these results are ruled by the Ostwald ripening mechanism, which is characteristic of colloidal synthesis like the one-pot method employed here.

Supplementary Information

Supplementary data are available free of charge at http://jbcs.sbq.org.br as PDF file.

Acknowledgments

This work was supported by Fundação de Amparo à Pesquisa do Estado de Minas Gerais (FAPEMIG), Conselho Nacional de Desenvolvimento Científico e Tecnológico (CNPq), Coordenação de Aperfeiçoamento de Pessoal de Nível Superior (CAPES) and Melt Metais & Ligas S. A.

References

1. Geiregat, P.; Justo, Y.; Abe, S.; Flamee, S.; Hens, Z.; *ACS Nano* **2013**, *7*, 987.
2. Hameau, S.; Guldner, Y.; Verzelen, O.; Ferreira, R.; Bastard, G.; Zeman, J.; Lemaitre, A.; Gerard, J. M.; *Phys. Rev. Lett.* **1999**, *83*, 4152.
3. Esteve-Turrillas, F. A.; Abad-Fuentes, A.; *Biosens. Bioelectron.* **2013**, *41*, 12.
4. Chan, W. C. W.; Nie, S. M.; *Science* **1998**, *281*, 2016.
5. Dahan, M.; Laurence, T.; Pinaud, F.; Chemla, D. S.; Alivisatos, A. P.; Sauer, M.; Weiss, S.; *Opt. Lett.* **2001**, *26*, 825.
6. Sargent, E. H.; *Nat. Photonics* **2012**, *6*, 133.
7. Vivas, M. G.; Cury, J. F.; Schiavon, M. A.; Mendonca, C. R.; *J. Phys. Chem. C* **2013**, *117*, 8530.

8. Larson, D. R.; Zipfel, W. R.; Williams, R. M.; Clark, S. W.; Bruchez, M. P.; Wise, F. W.; Webb, W. W.; *Science* **2003**, *300*, 1434.
9. Knowles, K. E.; Frederick, M. T.; Tice, D. B.; Morris-Cohen, A. J.; Weiss, E. A.; *J. Phys. Chem. Lett.* **2012**, *3*, 18.
10. Moreels, I.; Lambert, K.; Smeets, D.; De Muynck, D.; Nollet, T.; Martins, J. C.; Vanhaecke, F.; Vantomme, A.; Delerue, C.; Allan, G.; Hens, Z.; *ACS Nano* **2009**, *3*, 3023.
11. Pichaandi, J.; van Veggel, F. C. J. M.; *Coord. Chem. Rev.* **2014**, *263-264*, 138.
12. Keuleyan, S.; Lhuillier, E.; Guyot-Sionnest, P.; *J. Am. Chem. Soc.* **2011**, *133*, 16422.
13. Chuang, C.-H.; Burda, C.; *J. Phys. Chem. Lett.* **2012**, *3*, 1921.
14. Han, D.; Song, C.; Li, X.; *Mater. Chem. Phys.* **2009**, *116*, 41.
15. Han, D.; Song, C.; Li, X.; *J. Nanomater.* **2010**, *2010*, article ID 290763.
16. Li, M.; Yu, X.-F.; Liang, S.; Peng, X.-N.; Yang, Z.-J.; Wang, Y.-L.; Wang, Q.-Q.; *Adv. Funct. Mater.* **2011**, *21*, 1788.
17. Farias, P. M. A.; Fontes, A.; Galembeck, A.; Figueiredo, R. C. B. Q.; Santos, B. S.; *J. Braz. Chem. Soc.* **2008**, *19*, 352.
18. Nikesh, V. V.; Dharmadhikari, A.; Ono, H.; Nozaki, S.; Kumar, G. R.; Mahamuni, S.; *Appl. Phys. Lett.* **2004**, *84*, 4602.
19. Sousa, J. C. L.; Vivas, M. G.; Ferrari, J. L.; Mendonca, C. R.; Schiavon, M. A.; *RSC Adv.* **2014**, *4*, 36024.
20. Zhu, X.; Chen, L.; Shen, P.; Jia, J.; Zhang, D.; Yang, L.; *J. Agric. Food Chem.* **2011**, *59*, 2184.
21. Stanisavljevic, M.; Krizkova, S.; Vaculovicova, M.; Kizek, R.; Adam, V.; *Biosens. Bioelectron.* **2015**, *74*, 562.
22. Walcarius, A.; Minteer, S. D.; Wang, J.; Lin, Y.; Merkoci, A.; *J. Mater. Chem. B* **2013**, *1*, 4878.
23. Tang, W.; Zhu, G.; Liang, L.; Zhang, C.-Y.; *Analyst* **2015**, *140*, 5936.
24. Michalet, X.; Pinaud, F. F.; Bentolila, L. A.; Tsay, J. M.; Doose, S.; Li, J. J.; Sundaresan, G.; Wu, A. M.; Gambhir, S. S.; Weiss, S.; *Science* **2005**, *307*, 538.
25. Rosenthal, S. J.; Chang, J. C.; Kovtun, O.; McBride, J. R.; Tomlinson, I. D.; *Chem. Biol.* **2011**, *18*, 10.
26. Liu, W.; Howarth, M.; Greytak, A. B.; Zheng, Y.; Nocera, D. G.; Ting, A. Y.; Bawendi, M. G.; *J. Am. Chem. Soc.* **2008**, *130*, 1274.
27. He, H.; Feng, M.; Hu, J.; Chen, C.; Wang, J.; Wang, X.; Xu, H.; Lu, J. R.; *ACS Appl. Mater. Interfaces* **2012**, *4*, 6362.
28. Wang, Q.; Fang, T.; Liu, P.; Deng, B.; Min, X.; Li, X.; *Inorg. Chem.* **2012**, *51*, 9208.
29. Wang, Y.; Liu, S.; *J. Chil. Chem. Soc.* **2012**, *57*, 1109.
30. Grabolle, M.; Spieles, M.; Lesnyak, V.; Gaponik, N.; Eychmueller, A.; Resch-Genger, U.; *Anal. Chem.* **2009**, *81*, 6285.
31. Laverdant, J.; de Marcillac, W. D.; Barthou, C.; Chinh, V. D.; Schwob, C.; Coolen, L.; Benalloul, P.; Nga, P. T.; Maître, A.; *Materials* **2011**, *4*, 1182.
32. Vengrenovich, R. D.; Gudyma, Y. V.; Yarema, S. V.; *Semiconductors* **2001**, *35*, 1378.
33. Finsy, R.; *Langmuir* **2004**, *20*, 2975.
34. Kubin, R. F.; Fletcher, A. N.; *J. Lumin.* **1982**, *27*, 455.
35. Yu, W. W.; Qu, L. H.; Guo, W. Z.; Peng, X. G.; *Chem. Mater.* **2003**, *15*, 2854.
36. Mansur, H. S.; Mansur, A. A. P.; *Mater. Chem. Phys.* **2011**, *125*, 709.
37. Tauc, J.; Menth, A.; *J. Non-Cryst. Solids* **1972**, *569*, 8.
38 Green, M. J.; *Mater. Chem* **2010**, *20*, 5797.
39 Medintz, L.; Uyeda, H. T.; Goldman, E. R.; Mattoussi, H.; *Nat. Mater.* **2005**, *4*, 435.
40 Silva, F. O.; Carvalho, M. S.; Mendonça, R.; Macedo, W. A. A.; Balzuweit, K.; Reiss, P.; Schiavon, M. A.; *Nanoscale Res. Lett.* **2012**, *7*, 536.
41 Vale, B. R. C.; Vieira, K. O.; Sousa, J. C. L.; Ferrari, J. L.; Schiavon, M. A.; *Quim. Nova* **2015**, *38*, 22.
42. Zhao, D.; Fang, Y.; Wanga, H.; He, Z.; *J. Mater. Chem.* **2011**, *21*, 13365.
43. Sugimoto, T.; *Adv. Colloid Interface Sci.* **1987**, *28*, 65.
44. Demas, J. N.; Crosby, G. A.; *J. Phys. Chem.* **1971**, *75*, 991.
45. Zheng, Y.; Gao, S.; Ying, J. Y.; *Adv. Mater.* **2007**, *19*, 376.
46. Sousa, J. C. L.; Vivas, M. G.; Vale, B. R. C.; Ferrari, J. L.; Schiavon, M. A.; *J. Nanosci. Nanotechnol.* **2018**, *18*, 651.
47. Keller, H. R.; Massart, D. L.; *Chemom. Intell. Lab. Syst.* **1992**, *12*, 209.
48. Mutavdzic, D.; Xu, J.; Thakur, G.; Triulzi, R.; Kasas, S.; Jeremic, M.; Leblanc, R.; Radotic, K.; *Analyst* **2011**, *136*, 2391.
49. Atkins, P.; Overton, T.; Rourke, J.; Weller, M.; Armstrong, F.; *Inorganic Chemistry*, 5th ed.; Oxford University Press: New York, 2010.

Submitted: April 22, 2018
Published online: July 2, 2018